ISSN 2176-5480

22nd International Congress of Mechanical Engineering (COBEM 2013)
November 3-7, 2013, Ribeirão Preto, SP, Brazil

DYNAMIC BEHAVIOR OF TYPICAL ALUMINUM BOX BEAM UNDER COMPRESSION LOAD IN THE POST-BUCKLING REGIME

Felipe Franzoni[1]
Sérgio Frascino Müller de Almeida[2]
Instituto Tecnológico de Aeronáutica-ITA, CTA-ITA-IEM, Pça Mal. Eduardo Gomes, 50, CEP 12228-900, São José dos Campos-SP, Brasil
[1]franzoni@ita.br, [2]frascino@ita.br

Clóvis Augusto Eça Ferreira[3]
Instituto Tecnológico de Aeronáutica-ITA, CTA-ITA-IEM, Pça Mal. Eduardo Gomes, 50, CEP 12228-900, São José dos Campos-SP, Brasil
[3]eca@embraer.com.br

Abstract. *This paper describes an approach to identify the modal parameters (natural frequency and modal shape) of a typical aeronautical aluminum box beam in pre- and post-buckling regimes. The methodology is based on the tangent stiffness matrix originating from reduced dynamic models. To illustrate the proposed method, a numerical study using a commercial finite element package (Abaqus 6.11-1™) is performed. The numerical procedure considers a simply supported box beam under uniaxial compression load with different degrees of eccentricity in pre- and post-buckling regimes. In addition, a methodology based on regular solution of the commercial finite element package is performed considering geometrical nonlinearity. These models are adjusted for several levels of load in order to characterize the dynamic behavior of the structure during the loss of stability. The results of both methodologies are compared. The advantages and drawbacks of the proposed method are demonstrated through these numerical tests.*

Keywords: *box beam, nonlinear finite element method, post-buckling behavior and modal analysis.*

1. INTRODUCTION

Due to its high strength and lightweight, the box beam structures have been widely used in aeronautical, naval, civil and mechanical engineering applications. In particular, in aeronautical engineering, numerous main structures, *e.g.*, a typical aircraft wing can be simplistically modeled as a simple box beam structure. Nevertheless, a box beam is highly susceptible to vibration and local buckling phenomena.

These phenomena may occur simultaneously, since local buckling does not imply global failure of the structure. Together, they can induce large displacements, resonance, chaotic motion and dynamic snap-through between equilibrium states instigating several damages in structural mechanics (Boutyour, *et al*., 2006). Thus, it is crucial to predict with reasonable accuracy the dynamic behavior of a box beam component under local buckling phenomenon during the design phase. Although the importance of characterizing vibration of structures in the post-buckling regime, Mohri, *et al*. (2004) emphasize that most researches in this area are limited to the pre-buckling regime.

In order to overcome the drawbacks above, different strategies have been proposed to analyze the structural dynamic behavior in pre and post-buckling regime for several engineering applications. Chen and Virgin, 2005(a-b) proposed an asymptotic and non-stationary finite element procedure to obtain the pre and post-buckling static response while the dynamic behavior is obtained through an adaptive non-stationary load sweeping algorithm. Plates under generalized (mechanical and thermal) loading considering several boundary conditions are used to verify the methodology. The main advantage is the good characterization of the dynamic behavior before and after the mode jumping phenomenon, even for a highly nonlinear buckling behavior.

Boutyour, *et al*. (2006) also proposed an asymptotic numerical method for small vibration of post-buckled shell using a nonlinear geometrical formulation (large displacements and large rotations). The coupled static and dynamic problem is solved as a sequence of linear problems and the methodology is validated considering rectangular plates, thin and thick cylindrical roof and deep arches. The authors emphasizes that the load–frequency curves are obtained for various natural frequencies at any desired load level.

Mohri, *et al*. (2004) successfully employed a methodology based on a nonlinear model accounting for warping, bending–bending and torsion–bending couplings for the analysis of thin-walled structures with instabilities. Using the tangential stiffness matrix originating from the static equilibrium equations an eigenvalue problem is defined for small vibrations. Several thin-walled beams under both axial and lateral loads are investigated to support the formulation.

2. OVERVIEW OF THE METHODOLOGY

Finite element models with geometric nonlinearity formulation are developed using a commercial finite element package (Abaqus 6.11-1™). Firstly, the static equilibrium branches are computed using an incremental solution

ISSN 2176-5480

(Newton-Raphson's method) for 50 load steps; at each load step, a dynamic eigenvalue problem is solved yielding the frequencies and corresponding modal shapes. Secondly, considering 10 load steps, the nonlinear static problem is solved and for each equilibrium branch the Guyan-Irons reduction method is used through dynamic substructure generation in order to determine the reduced dynamic model. Another eigenvalue problem is solved in order to obtain the frequencies for the reduced model. Numerical tests are performed considering a typical aluminum box beam under compression load for several levels of eccentricities in pre and post-buckling regime.

2.1 Finite element incremental formulation

By discretizing the virtual work equation and defining the residual vector, the equilibrium equations originating from a nonlinear finite element problem can be described in terms of a few to thousands variables, Abaqus (2011):

$$R^n\left(u^m\right)=0 \tag{1}$$

where R^n is the force component conjugate to the n^{th} variable in the problem and u^m is the value of the m^{th} variable. Allowing for a history-dependent solution developed by an incremental formulation:

$$R^n\left(u_i^m+c_{i+1}^m\right)=0 \tag{2}$$

where u_i^m is an approximation for the solution after i iterations and c_{i+1}^m is the difference between this solution and the exactly solution. Considering an expansion in Taylor series about the approximated solution u_i^m and neglecting higher order terms:

$$\mathbf{K}_{T,i}^{nP}c_{i+1}^P=-R_i^n \tag{3}$$

where the Jacobian matrix and the residual vector, $\mathbf{K}_{T,i}^{nP}$ and R_i^n, are, respectively:

$$\mathbf{K}_{T,i}^{nP}=\frac{\partial R^n}{\partial u^P}\left(u_i^m\right) \tag{4}$$

$$R_i^n=R^n\left(u_i^m\right) \tag{5}$$

and the next approximated solution:

$$u_{i+1}^m=u_i^m+c_{i+1}^m \tag{6}$$

2.2 The dynamic equation around a deformed static equilibrium branch

Considering a static equilibrium state in pre or post-buckling regime the tangential stiffness matrix, Eq. (4), can be written as a summary of the following stiffness matrix, (Ferreira, 2007):

$$\mathbf{K}_T=\mathbf{K}_L+\mathbf{K}_R+\mathbf{K}_\sigma \tag{7}$$

where $\mathbf{K}_L$ is the usual stiffness matrix, $\mathbf{K}_R$ is the stiffness due to large rotations and $\mathbf{K}_\sigma$ is the geometric stiffness, which is function of the geometry and initial stress. Once the tangential stiffness is defined one can obtain the dynamic equations applying the Hamilton's principle, (Meirovitch, 1970):

$$\delta\int_{t_1}^{t_2}\left(\frac{1}{2}\{\dot{q}\}^T\mathbf{M}\{\dot{q}\}-\frac{1}{2}\{q\}^T\mathbf{K}_T\{q\}\right)dt=0 \tag{8}$$

where δ is the variational operator, $\bullet^T$ the transpose operator, dt a time increment, t_1 to t_2 a time interval, $\dot{q}$ and q are the velocity and displacement vectors, respectively, $\mathbf{M}$ is the mass matrix and its associated term the kinetic energy, $\mathbf{K}_T$ is the tangential stiffness, Eq. (7), and its associated term the work due to conservative forces. Once integrated, one can minimize the functional and found the given matrix differential equation:

ISSN 2176-5480

$$\mathbf{M}\{\ddot{q}\}+\mathbf{K}_T\{q\}=0 \tag{9}$$

Assuming the modal generalized displacement, (Bathe, 1996), Eq. (9) can be uncoupled and the vibration problem is summarized into the following eigenvalue equation:

$$\left(\mathbf{K}_T-\omega_n^2\mathbf{M}\right)\{\phi_n\}=0 \tag{10}$$

where the ω_n is the n^{th} natural frequency and $\{\phi_n\}$ is the n^{th} eigenvector (modal shape).

2.3 The Guyan-Irons reduction method

The free vibration problem modeled, Eq. (10), considering N degrees of freedom, is expressed by the following equivalent algebraic system, Sotiropoulos, 1984:

$$\left(\mathbf{K}_{N\times N}-\omega_n^2\mathbf{M}_{N\times N}\right)\{\phi_n\}_{N\times 1}=0 \tag{11}$$

where $\mathbf{K}_{N\times N}$ and $\mathbf{M}_{N\times N}$ are the stiffness and mass matrices and ω_n^2 and $\{\phi_n\}_{N\times 1}$ are the n^{th} eigenvalue and eigenvectors for the $N\times N$ system, respectively. In order to reduce the number of degrees of freedom from N to M, a vector $\{\phi_n\}_{M\times 1}$ included in the vector $\{\phi_n\}_{N\times 1}$ is defined and the Eq. (11) is rewritten as:

$$\left(\begin{bmatrix}\mathbf{K}_{MM} & \mathbf{K}_{MD}\\ \mathbf{K}_{DM} & \mathbf{K}_{DD}\end{bmatrix}-\omega_n^2\begin{bmatrix}\mathbf{M}_{MM} & \mathbf{M}_{MD}\\ \mathbf{M}_{DM} & \mathbf{M}_{DD}\end{bmatrix}\right)\begin{Bmatrix}\phi_M\\ \phi_D\end{Bmatrix}=0 \tag{12}$$

where M are the retained degrees of freedom and D are the eliminated degrees of freedom, $D=N-M$. According to the Guyan-Irons method the retained stiffness and mass matrices are given by, (Guyan, 1965) and (Irons, 1965):

$$\mathbf{K}_M^A=\mathbf{K}_{MM}-\mathbf{K}_{MD}\mathbf{K}_{DD}^{-1}\mathbf{K}_{DM} \tag{13}$$

$$\mathbf{M}_M^A=\mathbf{M}_{MM}-\mathbf{M}_{MD}\mathbf{K}_{DD}^{-1}\mathbf{K}_{DM}-\mathbf{K}_{MD}\mathbf{K}_{DD}^{-1}\left(\mathbf{M}_{DM}-\mathbf{M}_{DD}\mathbf{K}_{DD}^{-1}\mathbf{K}_{DM}\right) \tag{14}$$

where the superscript A indicates an approximation, since the method is not exact and depends on the evaluated frequency range. According to Eq. (10) one can write the reduced dynamic problem, (Sotiropoulos, 1984):

$$\left(\left(\mathbf{K}_T\right)_{M\times M}^A-\omega_n^2\mathbf{M}_{M\times M}^A\right)\{\phi_n\}_{M\times 1}=0 \tag{15}$$

where $\left(\mathbf{K}_T\right)_{M\times M}^A$ is the reduced tangential stiffness matrix and $\mathbf{M}_{M\times M}^A$ is the reduced mass matrix.

3. THE FINITE ELEMENT MODEL SETUP

This section presents the finite element model setup used to illustrate the proposed approach. The box beam structure analyzed consists of: six ribs (1), two stringers (2) and two skins (3), and is depicted in Fig. 1.

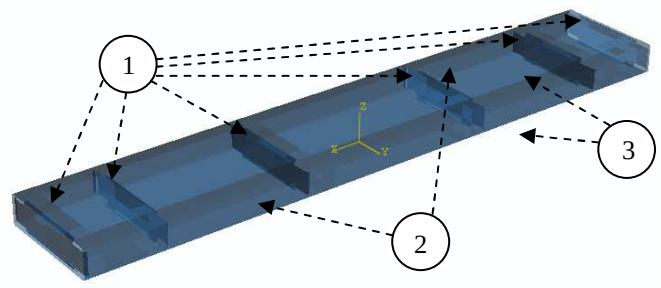

Figure 1. Geometry of the model.

ISSN 2176-5480

As the main purpose of the model is to represent the local buckling phenomenon of the skin and the global and local frequencies of the whole structure, a simplified geometry was created. Initially, all parts were designed separated and assembled together considering an average thickness of the box beam section. Then, a geometry merge procedure was performed and a new geometry was created. The dimensions of the geometry are presented in Tab. 1 and the aluminum properties considered in the analysis in Tab. 2, (MMPDS-01, 2003).

Table 1. Geometrical properties.

Description	Value	Units
Total width (external)	158,60	mm
Total height	41,00	mm
Total length	900,00	mm
Stringer and ribs thickness	1,30	mm
Skin thickness	1,00	mm
Distance between centralized ribs (between rivets)	259,40	mm
Distance between the extremity ribs (between rivets)	84,13	mm
Bending radius (internal)	3	mm

Table 2. Material properties.

Variable	Description	Value	Units
E	Elastic modulus, MMPDS-01 (2003)	72394,97	MPa
E	Elastic modulus, (Ramber-Osgood model)	73676,95	MPa
υ	Poisson ratio	0,33	-
ρ	Density	2780×10^{-12}	ton/mm^3
F_{cy}	Compressive yield stress	275,79	MPa
n	Ramberg-Osgood parameter	15	-

Once the geometry is defined, it can be partitioned, so the total thickness of each region may be assigned. A structured algorithm considering minimum mesh transition and quadrilateral shape is used in order to mesh the geometry. The chosen element is the S4R (4-node, reduced integration) shell element with 5 points of integration through its thickness. After a preliminary study, a kinematic constrained coupling is used in order to model the support devices of the box beam and apply the uniaxial load (with or without eccentricity). The use of the control points does not affect significantly the global modal results (the highest deviation is about 7% for 63 mm of eccentricity). Figure 2 presents the eccentricity levels considered: no eccentricity, 21 mm, 42 mm and 63 mm, respectively, moreover one can see the details about the control points.

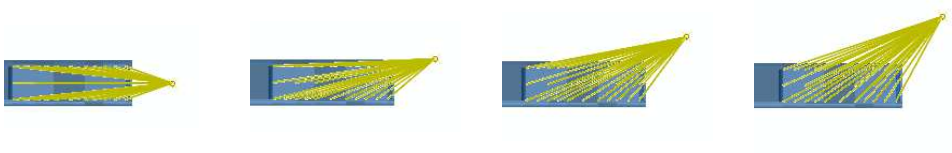

Figure 2. Eccentricity levels considered.

In order to determine a reasonable size for the shell element a convergence analysis is performed by defining two new models. The analysis is performed considering the central and the lateral panel, both with simple supported boundary conditions, that have been verified for **(i)** linear buckling and **(ii)** linear modal analysis. The results are presented in Tables 3 and 4.

Table 3. Convergence analysis – central panel.

Element size [mm]	P_1 [kN]	P_2 [kN]	P_3 [kN]	P_4 [kN]	f_1 [Hz]	f_2 [Hz]	f_3 [Hz]
25	2129.1	2596	3418.4	3845.4	395.62	497.76	720.65
12.5	2021.1	2392.3	3173.3	3252.4	364.34	468.93	663.69
6.25	1994.9	2349.2	3113.8	3145.4	357.21	462.36	651.96
3.125	1989.2	2339.3	3101.1	3120.5	355.69	460.91	649.2
1.5625	1987.8	2336.8	3098.0	3114.2	355.31	460.55	648.5

ISSN 2176-5480

Table 4. Convergence analysis – lateral panel.

Element size [mm]	P_1 [kN]	P_2 [kN]	P_3 [kN]	P_4 [kN]	f_1 [Hz]	f_2 [Hz]	f_3 [Hz]
25	2165.9	2968.1	2970.7	4816.2	194.69	337.55	607.59
12.5	2052.7	2677.6	2769.8	3863	189.76	327.95	564.38
6.25	2025.3	2613.1	2721.6	3680.3	188.53	325.54	555.48
3.125	2019.2	2598.8	2711.2	3640.7	188.26	324.99	553.23
1.5625	2017.7	2595.2	2708.7	3631	188.19	324.85	552.67

A deviation is calculated for every additional refinement between two successive sizes:

$$e = 100\left(\frac{g_{i+1}}{g_i} - 1\right) \tag{16}$$

where g_{i+1} is new result for the control variable (buckling load or natural frequency) and g_i is the previous value for the same variable. Figures (3-6) show the error variation for each controlled variable through successive refinements.

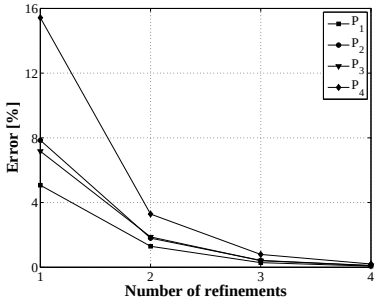

Figure 3. Deviation of buckling load – central panel.

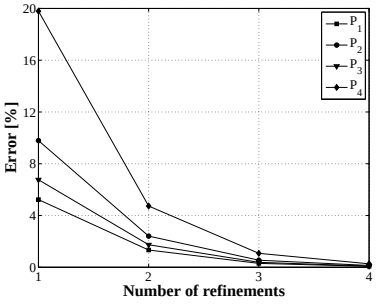

Figure 4. Deviation of buckling load – lateral panel.

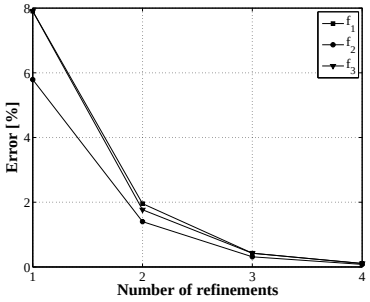

Figure 5. Deviation of natural frequencies – central panel.

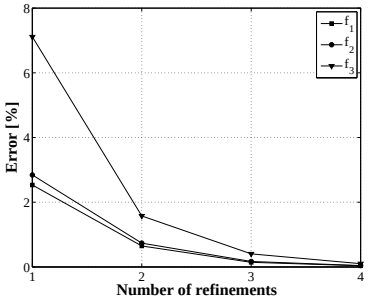

Figure 6. Deviation of natural frequencies – lateral panel.

Analyzing Figures (3-6) one can notice that the fourth refinement results in negligible improvement. Therefore, the chosen element size is 3.125 mm (for the panel). In addition, for the stringers and ribs regions a refined mesh is not necessary because they do not buckle, hence it is used 6 elements through ribs and stringer height. On the other hand, 8 elements are used in curved regions to avoid stress concentration. Figure 7 presents a cut around the bottom symmetric plane of the meshed geometry (48316 elements; 48462 nodes).

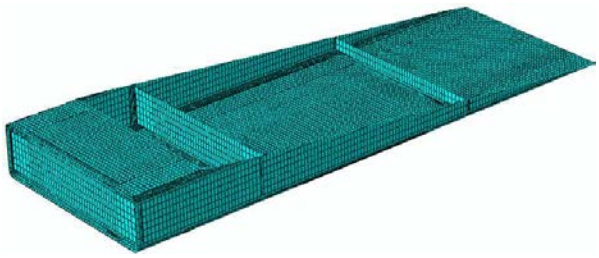

Figure 7. Cut of the meshed geometry.

ISSN 2176-5480

Aiming at determining the reduced dynamic model, several nodes are chosen on both sides of the box beam mesh (total of 302 nodes). Figure 8 shows the chosen nodes for one side (the other side is symmetric). The retained degree of freedom for each chosen node is the out of plane displacement u_3. The methodology based on the reduced dynamic models is verified for 10 load steps, Tab. 5.

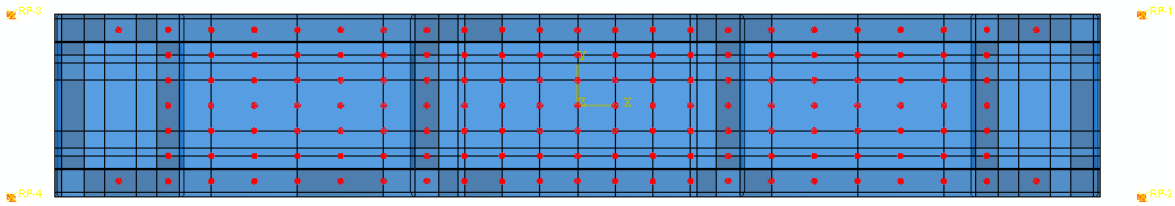

Figure 8. Retained nodes.

Table 5. Chosen load steps.

No eccentricity		21 mm		42 mm		63 mm	
F [kN]	w [mm]	F [kN]	w [mm]	F [kN]	w [mm]	F [kN]	w [mm]
2	0.041	2	0.096	1	0.131	1	0.270
4	0.082	3	0.145	1.7	0.224	1.5	0.404
6	0.123	4	0.195	2.4	0.317	2	0.542
8	0.164	5	0.245	3.1	0.413	2.5	0.680
10	0.205	6	0.296	3.8	0.508	3	0.820
12	0.245	7	0.348	4.5	0.606	3.5	0.963
14	0.287	8	0.409	5.2	0.717	4	1.130
16	0.328	9	0.479	5.9	0.845	4.5	1.311
18	0.379	10	0.552	6.6	0.978	5	1.498
20	0.433	11	0.628	7.3	1.116	5.5	1.691
22	0.487	12	0.707	8	1.258	6	1.889

4. NUMERICAL RESULTS

This section presents the numerical results for both methodologies proposed in this paper. First, one can see the solution for the nonlinear static problem considering geometric nonlinearity. This static solution is used as several equilibrium states to solve the dynamic problems being required by both methodologies.

4.1 Static nonlinear analysis

The nonlinear static problem is solved through Newton's iterative method considering the load applied through displacement control. A time increment of 0.01 s is considered and the time period is defined as 1 s. The total displacement for each eccentricity is chosen using a preliminary model accounting nonlinear material behavior (Ramberg-Osgood plastic model) to ensure that the complete numerical test is within the elastic range, Figures (9-12).

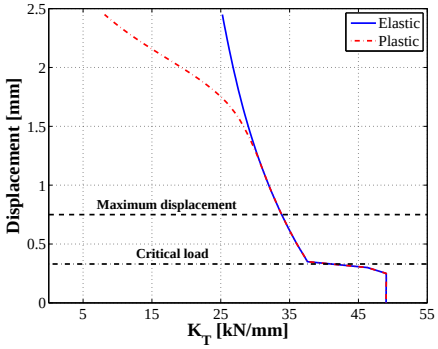

Figure 9. Equilibrium chart – no eccentricity.

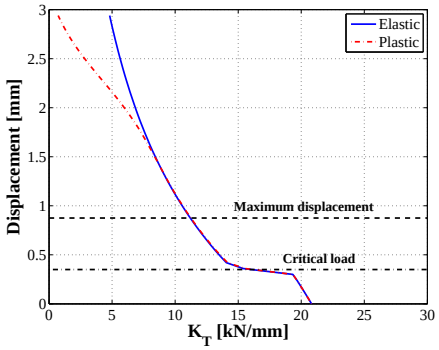

Figure 10. Equilibrium chart – 21 mm.

ISSN 2176-5480

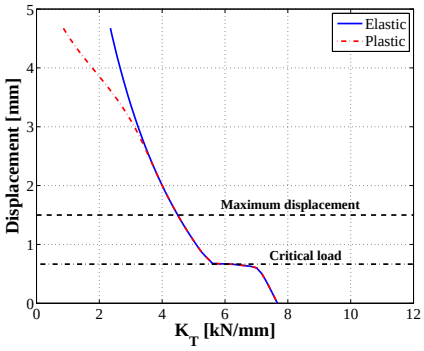

Figure 11. Equilibrium chart – 42 mm.

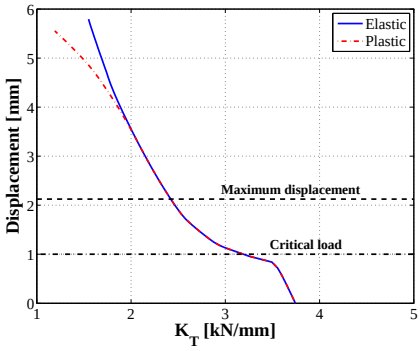

Figure 12. Equilibrium chart – 63 mm.

In Figures (8-11) one may notice that the equilibrium plot for tangential stiffness (with respect to the control points) comparing the elastic and plastic response for all considered eccentricities. Moreover, the chosen total displacement and the critical load (determined through an eigenvalue problem) are presented (also in Tab. 6 for a better evaluation).

Table 6. Total displacement and linear buckling analysis results.

Boundary condition [mm]	P_1 [N]	Equivalent displacement [mm]	Total displacement [mm]
No eccentricity	15991	0.33	0.75
21	7570.6	0.35	0.875
42	4909.3	0.67	1.5
63	3632.2	1.00	2.125

4.2 Pre and post-buckling dynamic analysis

In order to describe the frequency variation of the box beam in pre and post-buckling regime, the static results presented before are divided into 50 equilibrium branches and each one is used as initial state for vibration models, Eq. 11, which is solved through Lanczos algorithm. Figures (13-15) present the variation of the 1st, 2nd and 3rd modes due to the loss of stability for each considered boundary condition – the loaded modal shape presented is with total load.

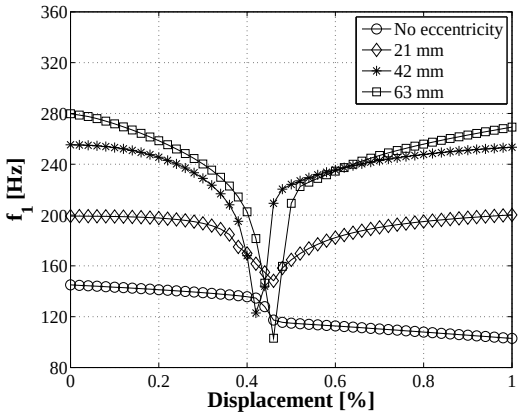

a) Frequency variation – f_1.

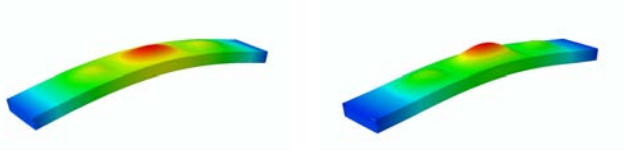

b) No eccentricity – unloaded.

c) 21 mm – unloaded.

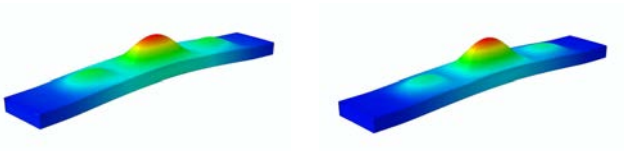

d) 42 mm – unloaded.

e) 63 mm – unloaded.

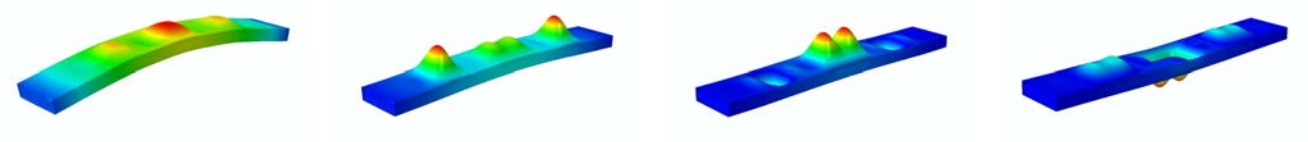

f) No eccentricity – loaded.

g) 21 mm – loaded.

h) 42 mm – loaded.

i) 63 mm – loaded.

Figure 13. Frequency and modal shape variation of the first mode – f_1, ϕ_1.

ISSN 2176-5480

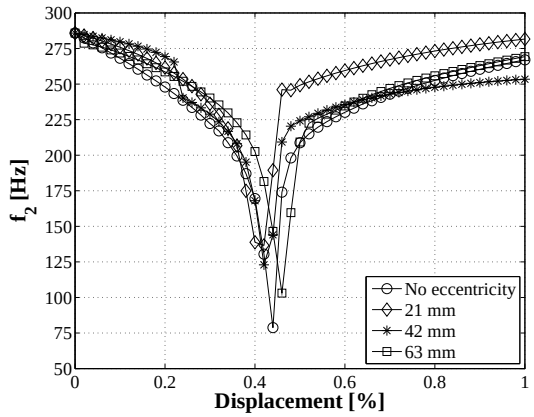

a) Frequency variation – f_2.

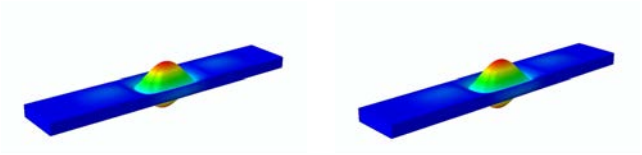

b) No eccentricity – unloaded.

c) 21 mm – unloaded.

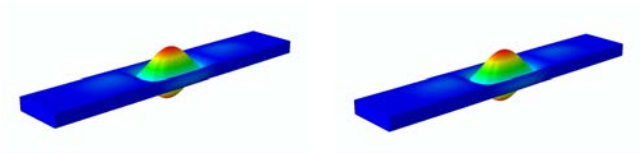

d) 42 mm – unloaded.

e) 63 mm – unloaded.

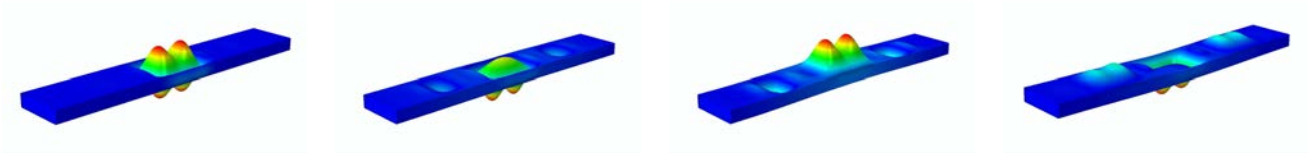

f) No eccentricity – loaded.

g) 21 mm – loaded.

h) 42 mm – loaded.

i) 63 mm – loaded.

Figure 14. Frequency and modal shape variation of the second mode – f_2, ϕ_2.

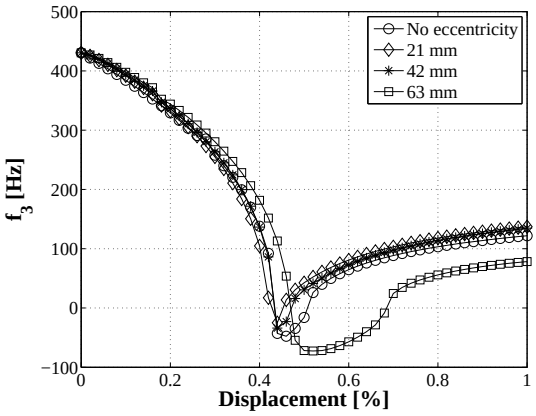

a) Frequency variation – f_3.

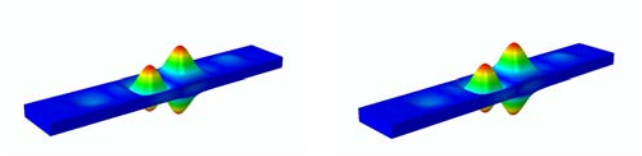

b) No eccentricity – unloaded.

c) 21 mm – unloaded.

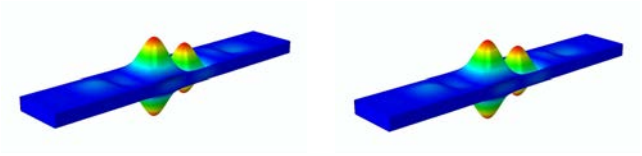

d) 42 mm – unloaded.

e) 63 mm – unloaded.

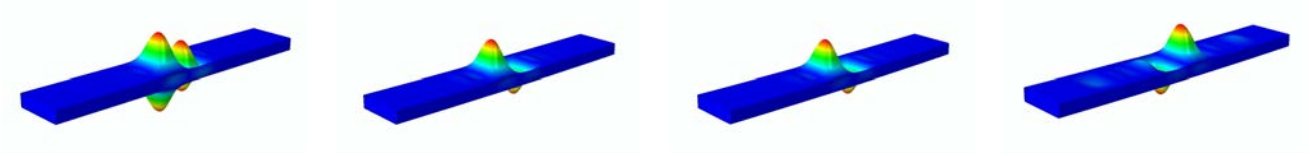

f) No eccentricity – loaded.

g) 21 mm – loaded.

h) 42 mm – loaded.

i) 63 mm – loaded.

Figure 15. Frequency and modal shape variation of the second mode – f_3, ϕ_3.

On the other hand, Figures (16-19) present the frequency variation considering each boundary condition separated. One can see the mode jumping effect between the second and third modes for all boundary conditions and the merge point between the first (global mode) and second (local mode) for 42 and 63 mm of eccentricity, respectively, generating a new mode called f_{12}, which is the result of the coalescence of both modes.

ISSN 2176-5480

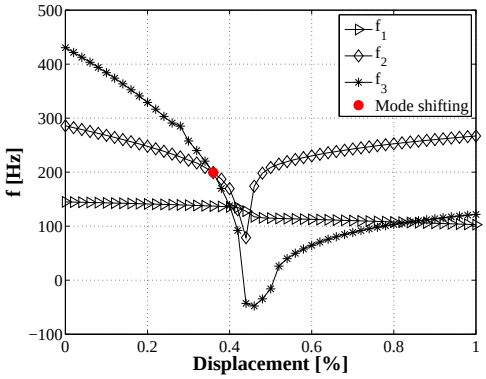

Figure 16. Frequency variation – no eccentricity.

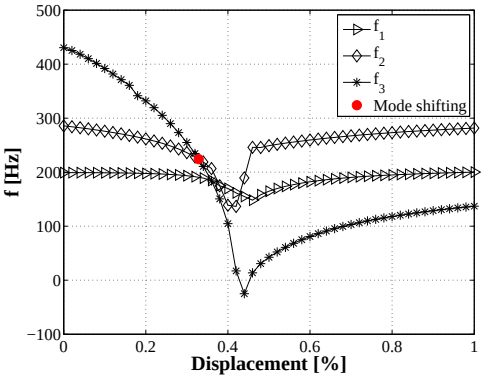

Figure 17. Frequency variation – 21 mm.

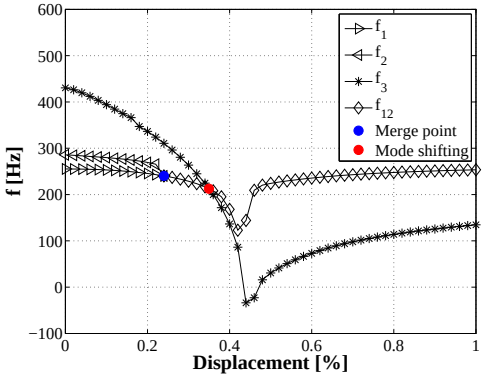

Figure 18. Frequency variation – 42 mm.

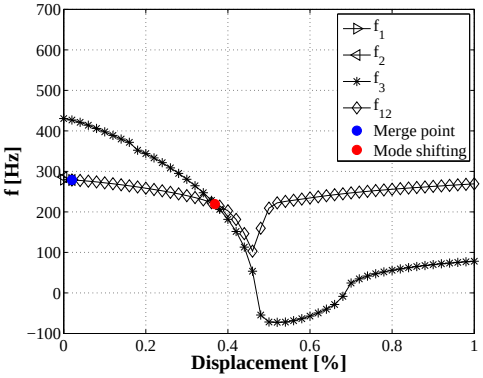

Figure 19. Frequency variation – 63 mm.

4.3 Pre and post-buckling dynamic analysis through reduced models

For each load step presented before, Tab. 5, reduced tangential stiffness and mass matrices are generated and the eigenvalue problem, Eq. (15), is solved with an algorithm implemented in Matlab™. Figures (20-23) show a comparison between the results from regular finite element solution presented on last section and the results from reduced dynamic models.

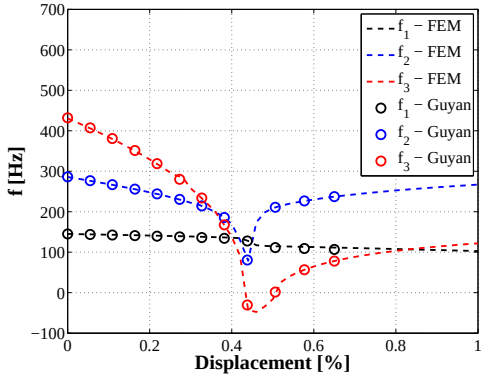

Figure 20 Frequency variation – no eccentricity.

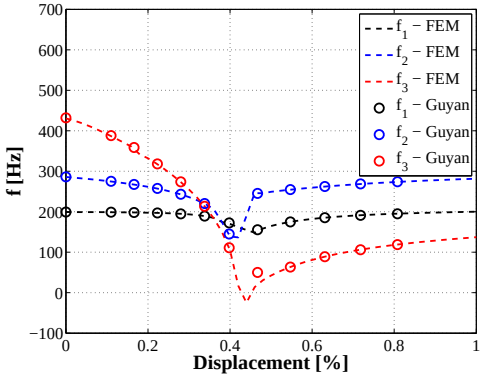

Figure 21. Frequency variation – 21 mm.

ISSN 2176-5480

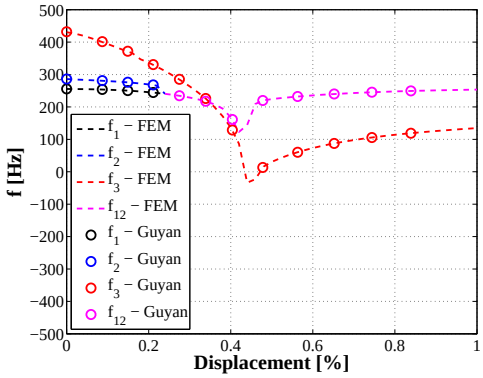

Figure 22. Frequency variation – 42 mm.

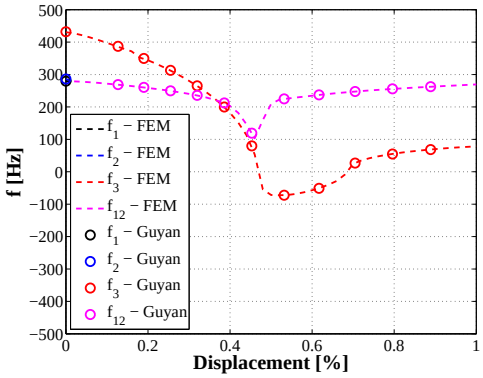

Figure 23. Frequency variation – 63 mm.

In order to verify the accuracy of the mode shapes presented in Figures (13-19) and (20-23) a Modal Assurance Criterion – MAC, LMS (2000), is computed (considering only degrees of freedom under compression) to quantify if there is a linear dependence between two eigenvectors from different load steps:

$$MAC_{jl,n} = \frac{\left|\left\{\phi_{j,n}\right\}^H \left\{\phi_{l,n}\right\}\right|^2}{\left(\left\{\phi_{j,n}\right\}^H \left\{\phi_{j,n}\right\}\right)\left(\left\{\phi_{l,n}\right\}^H \left\{\phi_{l,n}\right\}\right)} \tag{17}$$

where n is the mode index, ϕ_j is the j^{th} eigenvector, ϕ_l is the l^{th} eigenvector, $\bullet^H$ the transpose conjugate operator. Figures (24-27) present the results for all considered boundary conditions. The *MAC* index is computed for each mode with respect to the respective non-loaded eigenvector. A *MAC* index around 1 is expected for linear dependent eigenvectors whereas a value around 0 is expect for linear independent eigenvectors.

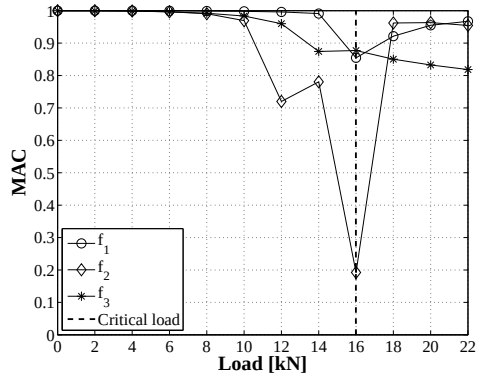

Figure 24. *MAC* analysis – no eccentricity.

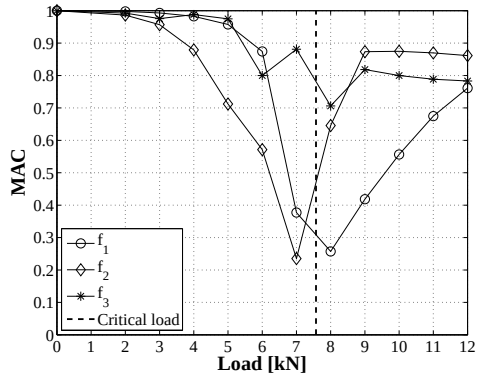

Figure 25. *MAC* analysis – 21 mm.

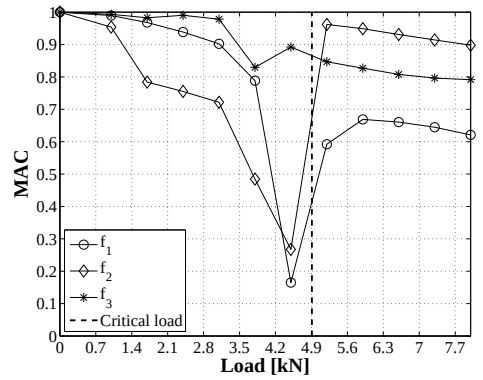

Figure 26. *MAC* analysis – 42 mm.

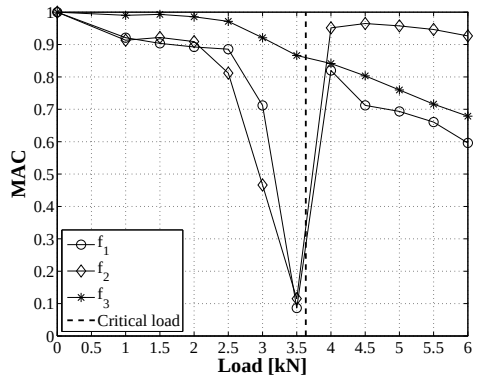

Figure 27. *MAC* analysis – 63 mm.

ISSN 2176-5480

5. FINAL REMARKS

A numerical approach to describe the frequency and mode shape variation of a box beam under uniaxial load considering an arbitrary eccentricity level was proposed in this paper. A reduced dynamic model was defined for several load steps using Guyan-Irons procedure. The associated dynamic eigenvalue problem is then solved in order to obtain the natural frequencies and modal shapes of the box beam during the loss of the stability. The results were compared with the usual finite element solution.

Both methodologies were able to detect the mode shifting between the second and third modes as well as to detect the merge between the first (global mode) and the second (local mode) modes. The MAC index results, Figures (24-27), enforce the merge between local and global modes, since the new coupled mode is not linearly independent from the original global and local modes. This indicates a coalescence of both modes. For all boundary conditions considered, the third natural frequency presented negative values near the linearized buckling load; according to Lyapunov stability criteria these negative values indicate an unstable response of the system.

The authors point out three conclusions aspects in this numerical approach for practical applications: **(i)** The numerical results obtained suggest the possibility to experimentally characterize the dynamic behavior through a static perturbation experiment; **(ii)** The eccentricity condition causes the merge between local and global modes and hinders the modal shape discrimination; **(iii)** The local buckling phenomenon effect on the global behavior of the box beam depends on the degree of merging between global and local modes.

The next step in this research work is the evaluation of the initial imperfection effect on the static equilibrium branches and, consequently, on the modal parameters results. Once included this effect, experimental tests can be performed and, subsequently, the validation of both finite element based on methodologies. Another aspect to explore is the validation of these procedures for composite material panels.

6. ACKNOWLEDGEMENTS

The authors would like to thank the support provided by Aeronautics Institute of Technology – ITA and National Council for Scientific and Technological Development (CNPq/Brazil). Sérgio Frascino Müller de Almeida and Felipe Franzoni are thankful the CNPq for their financial support, grants 303799/2010-2 and 132652/2012-9, respectively.

7. REFERENCES

Abaqus, 2011. *Abaqus 6.11 – Theory Manual*. Dassault Systèmes©.

Bathe, K-J., 1996. "*Finite Element Procedures*". Prentice Hall, Upper Saddle River, New Jersey, 1st edition.

Boutyour, E. H., Azrar, L. and Potier-Ferry, M., 2006. "Vibration of buckled elastic structures with large rotations by an asymptotic numerical method". *Composite and Structures*, Vol. 84, p. 93-101.

Chen, H. and Virgin, L. N., 2006a. "Finite element analysis of post-buckling dynamics in plates – Part I: An asymptotic approach". *International Journal of Solids and Structures*, Vol. 43, p. 3983-4007.

Chen, H. and Virgin, L. N., 2006b. "Finite element analysis of post-buckling dynamics in plates – Part II: A non-stationary analysis". *International Journal of Solids and Structures*, Vol. 43, p. 4008-4027.

Ferreira, C. A. E., 2007. *Pós-flambagem de Vigas Caixão Co-curadas*. M.Sc. thesis, Instituto Tecnológico de Aeronáutica, São José dos Campos.

Guyan, R. J., "Reduction of Stiffness and Mass Matrices". *AIAA Journal*, Vol. 3, n. 2, p. 380.

Irons, B. 1965. "Structural Eigenvalue Problems: Elimination of Unwanted Variables". *AIAA Journal*, Vol. 3, n. 5, p. 961-962.

LMS, 2000. *The LMS Theory and Background Book*. LMS International©.

Meirovitch, L., 1970. "*Methods of Analytical Dynamics*". Dover Publications, New York, 1st edition.

MMPDS-01, 2003. *Metallic Materials Properties Development and Standardization (MMPDS)*. U.S. Department of Transportation / Federal Aviation Administration / Office of Aviation Research, Washington.

Mohri, F., Azrar, L. and Potier-Ferry, M., 2004. "Vibration analysis of buckled thin-walled beams with open sections". *Journal of Sound and Vibration*, Vol. 275, p. 434-446.

Sotiropoulos, G, H., 1984. "Dynamic Reduction Algorithms for the Structural Eigenproblem", *Acta Mechanica*, Vol. 50, p. 231-248.

8. RESPONSIBILITY NOTICE

The authors are the only responsible for the printed material included in this paper.